


Article

Enrichment Characteristics and Mechanisms of Lithium, Gallium, and Rare Earth Elements (REY) within Late Permian Coal-Bearing Strata in Wanfu Mine, Xian'an Coalfield, Guangxi Province, Southwest China

Degao Zhang ^{1,2,3}, Xiaoyun Yan ^{1,2,3,*} , Baoqing Li ⁴, Jie Sun ¹, Li Zhang ¹, Xiangcheng Jin ⁵, Xiaotao Xu ¹, Shaobo Di ¹ and Shaoqing Huang ¹

¹ General Prospecting Institute of China National Administration of Coal Geology, Beijing 100039, China

² China National Administration of Coal Geology, Beijing 100038, China

³ Key Laboratory of Transparent Mine Geology and Digital Twin Technology, National Mine Safety Administration, Beijing 100039, China

⁴ Key Laboratory of Tectonics and Petroleum Resources, China University of Geosciences, Ministry of Education, Wuhan 430074, China

⁵ College of Geoscience and Survey Engineering, China University of Mining and Technology, Beijing 100083, China

* Correspondence: xyun.yan@outlook.com

Abstract: The study of lithium (Li), gallium (Ga), and rare earth elements (REY) within coal-bearing strata represents a cutting-edge concern in coal geology, ore deposit studies, and metallurgy research. With the rapid advancement of technology and emerging industries, the global demand for Li-Ga-REY has significantly escalated. Several countries worldwide are facing immense pressure due to shortages in Li-Ga-REY resources. Coal-associated Li-Ga-REY depositions have emerged as a pivotal direction for augmenting Li-Ga-REY reserves. To ascertain the enrichment distribution patterns and genetic mechanisms of Li-Ga-REY within the coal-bearing strata of the late Permian Heshan Formation in Wanfu mine, Xian'an Coalfield, Guangxi Province, this study carried out comprehensive testing and analysis on Li-Ga-REY enriched in the mineralized layers within the strata. The Heshan Formation in Wanfu mine presents four layers of Li-Ga-REY-enriched mineralization, labeled from bottom to top as mineralized layers I, II, III, and IV, corresponding to coal seams K5, K4, K3, and K2. These critical metals are predominantly hosted within clay minerals (kaolinite, illite/smectite, and chlorite). The enrichment of critical metals within the Heshan Formation is closely related to terrigenous detrital materials from the Daxin paleocontinent, volcanic detrital materials induced by the Emeishan mantle plume and the Yuenan magmatic arc. The accumulation of Li-Ga-REY and other critical elements within the mineralized layers is the result of inputs from terrestrial and volcanic detrital sources, interactions between peatification and diagenesis stages, and occasionally the input of metal-enriched fluids. In the mineralized layers I, II, and III, the content of lithium oxide (Li₂O) surpasses the boundary grade, and the levels of REY, Ga, and (Nb,Ta)₂O₅ are close to boundary grades, indicating promising exploration prospects. The Wanfu mine in the Xian'an Coalfield can be considered a primary target zone for the exploration and development of coal-associated critical metal resources in Guangxi.

Keywords: late permian; critical metal element; Xian'an coalfield; enrichment characteristic



Citation: Zhang, D.; Yan, X.; Li, B.; Sun, J.; Zhang, L.; Jin, X.; Xu, X.; Di, S.; Huang, S. Enrichment Characteristics and Mechanisms of Lithium, Gallium, and Rare Earth Elements (REY) within Late Permian Coal-Bearing Strata in Wanfu Mine, Xian'an Coalfield, Guangxi Province, Southwest China. *Minerals* **2024**, *14*, 853. <https://doi.org/10.3390/min14090853>

Academic Editor: Thomas Gentzis

Received: 25 April 2024

Revised: 10 August 2024

Accepted: 12 August 2024

Published: 23 August 2024



Copyright: © 2024 by the authors. Licensee MDPI, Basel, Switzerland. This article is an open access article distributed under the terms and conditions of the Creative Commons Attribution (CC BY) license (<https://creativecommons.org/licenses/by/4.0/>).

1. Introduction

Critical elements resources are dominated by rare metals (such as Li, Rb, and Zr), sparse metals (such as Ga, Ge, and Re), and rare earth elements (REY) [1,2]. Due to their unique material properties, critical elements play an irreplaceable role in emerging industries, including new materials, new energy, national defense, and military industries [3,4].

With the increasing shortage of conventional ore resources and the rapid growth of global demand, there is an urgent need to find and develop new resources for these elements. As a special sedimentary organic rock, coal can be enriched in critical elements and form large or super-large ore deposits under some specific geological conditions [5]. Therefore, the critical metal resources in coal-bearing strata can serve as an important supplement to conventional ore resources. The critical metal deposits discovered in coal-bearing strata include coal-Ge, coal-Ga-Al, and coal-REE [6–8].

The coal-bearing strata of the Heshan Formation in Late Permian Guangxi are mainly distributed in central and southwest Guangxi, including the Heshan, Xianyin, Fusui, Yishan, Binlin, Qianjiang, Xincheng and Baiwang coalfields [9]. Some studies have shown that critical elements are also enriched in some coal-bearing strata of the Heshan Formation in the Late Permian in Guangxi, such as the abnormal enrichment of V-Se-Mo-Re-U in the Late Permian coal measures in the Yishan coalfield. Dai et al. [10] and Shao et al. [11] found the enrichment of V-Se-Mo-U in the Late Permian coal measures in the Heshan Coalfield. Dai et al. [12], Liao Jialong et al. [9], and Zhang et al. [13] discovered the accumulation and mineralization of Li-Ga-REY in the late Permian coal measures in the Fusi and Xian’an coalfields. However, there are divergences about their occurrence states and material sources. On this basis, this paper takes the Li-Ga-REY-enriched mineralized layers in the Late Permian Heshan Formation in Wanfu mine, Xian’an Coalfield, as the research object to investigate critical elements and enrichment causes in coal-bearing strata, aiming to promote the exploration of critical metal depositions in the coal-bearing strata in Guangxi Province.

2. Geological Setting

The Wanfu mine, Xian’an Coalfield, Guangxi Province, is located on the western flank of the Xian’an syncline in the eastern part of the Youjiang Basin (Figure 1). Its central region consists of Middle Triassic argillaceous sandstone interbedded with mudstone, and Lower Triassic formations are composed of limestone, dolomite, calcareous sandstone, argillaceous sandstone, marl, and oolitic limestone [14]. The peripheral zones contain Upper Permian limestone, carbonaceous mudstone, coal, bauxite, and Middle–Lower Permian carbonate rocks. Additionally, exposures of the Devonian and Carboniferous systems are also presented in the region.

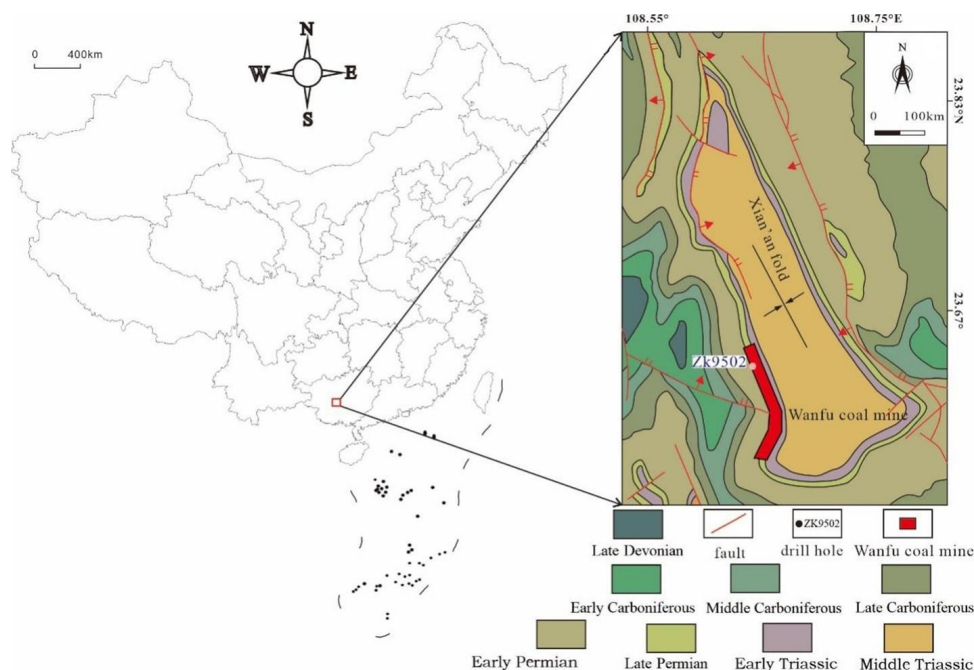


Figure 1. Regional geological map of the Wanfu mining, Xian’an coalfield, Guangxi Province.

Among them, the Late Permian Heshan Formation is the major coal-bearing stratum exhibiting littoral or marine–continental transitional facies. The coal-bearing stratum of the Heshan Formation is mainly composed of carbonate rock, carbonaceous mudstone, mudstone, marl and coal seam, and partial siltstone. Local parts have intercalations of medium–thick bedded argillaceous limestone, dolomite, or dolomitic limestone. Heshan Formation is in parallel unconformity contact with the lower Maokou Formation and in conformity contact with the overlying Dalong Formation (Figure 2) [15,16]. At the turn of the Middle and late Permian, influenced by the convergence of the Gondwana plate and Laua plate, the global sea level dropped, and the Emeishan basalt erupted, resulting in significant changes in the distribution pattern of sedimentary facies of the Heshan Formation, forming a composite of rifted basin and terrigenous clastic basin. The source regions of the Late Permian coal-bearing rock series in Guangxi are the Yunkai Upland, the Neozoic Upland, and the Jiangnan Upland, which had been formed.

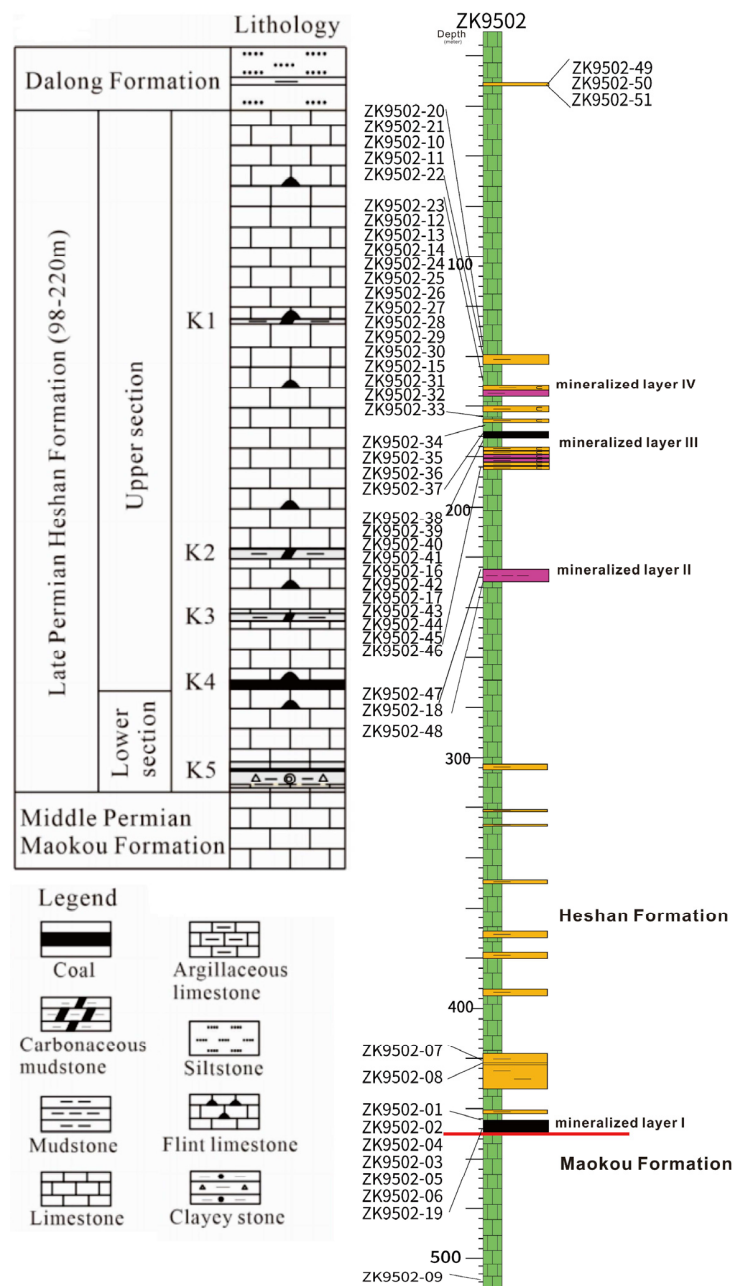


Figure 2. Sampling location map of borehole ZK9502 in the Wanfu mine, Xian’an coalfield, Guangxi Province.

3. Samples and Analytical Procedures

A total of fifty-one non-coal samples were collected from 9502 drill cores in the Wanfu mine, Xian'an Coalfield, Guangxi Province. In order to avoid contamination and oxidation, the samples collected from each ply were immediately stored in clean and uncontaminated plastic bags.

The trace element concentrations in the samples were determined by Agilent 7700e inductively coupled plasma mass spectrometry (ICP-MS, Agilent, Santa Clara, CA, USA). All samples were ashed at 900 °C. The high-temperature ashes (HTAs) were then analyzed by X-ray fluorescence spectrometry (XRF, ZSX Primus II, Rigaku, Tokyo, Japan) in order to determine the concentrations of major elements.

In order to identify the mineral assemblages in the study sample, a low-temperature oxygen-plasma asher (EMITECH K1050X, East Sussex, UK) was used to remove the organic matter from the coal. The coal low-temperature ash (LTA) and non-coal samples were analyzed using a Bruker D8 Advance XRD (Bruker, Leipzig, Germany). The sample was placed into a glass holder and gently pressed with a glass slide to minimize preferred orientation effects. A Bruker D8 Advance diffractometer was employed to obtain X-ray powder diffractograms with Ni-filtered Cu-K α radiation operated at 150 Kv and 40 mA from 5.0 to 90° with a step size of 0.02°.

After coating selected polished pellets with carbon, this study conducted mineral phase and element distribution analysis on them using a scanning electron microscope equipped with an energy-dispersive X-ray spectrometer (SEM-EDS, FEI Quanta™ 650 FEG, Eugene, OR, USA). A double polarizing microscope was employed to examine thin sections petrographically using microscopic techniques.

4. Results

4.1. Mineralogy

4.1.1. Minerals in Samples

The main crystalline phases in the samples identified by XRD are listed in Table 1. The mineral assemblages in the samples are kaolinite, illite, quartz, calcite, pyrite, albite (Table 1), and trace amounts of anatase, bassanite, chlorite, dolomite, diaspore, and anhydrite (Figure 3). Melanterite only exists in the sample ZK9502-14 (Table 1). The types of mineral assemblage of the four mineralized layers exhibit significant differences (Table 1). The minerals in the mineralized layer I (ZK9502-02,03,04,05,06) consist mainly of illite, calcite, pyrite, cookeite, and, to a lesser extent, albite and diaspore, along with trace amounts of kaolinite, dolomite, bassanite, rutile, and anatase. The minerals in the mineralized layer II (ZK9502-18) consist mainly of kaolinite, and, to a lesser extent, pyrite, along with trace amounts of calcite, dolomite, and anatase. The minerals in the mineralized layer III (ZK9502-16,42,17,43) consist mainly of kaolinite and quartz, and, to a lesser extent, clinocllore, illite, and calcite, along with trace amounts of pyrite, diaspore, bassanite, and anatase. The minerals in the mineralized layer IV (ZK9502-12,13,14) consist mainly of kaolinite, quartz, calcite, pyrite, and, to a lesser extent, dolomite, along with trace amounts of bassanite, anatase, and melanterite.

Table 1. Quantitative mineralogical composition of study samples (wt. %) determined using XRD.

| Sample | Illite | Kaolinite | Clinochlore | Cookeite | Quartz | Calcite | Dolomite | Siderite | Pyrite | Albite | Anatase | Rutile | Diaspore | Bassanite | Melanterite |
|-----------|--------|-----------|-------------|----------|--------|---------|----------|----------|--------|--------|---------|--------|----------|-----------|-------------|
| ZK9502-01 | | | | | | 95.10 | 1.10 | | 3.70 | | | | | | |
| ZK9502-02 | 37.00 | 2.90 | | | | 20.50 | 1.70 | | 28.70 | | 0.90 | | 4.70 | 3.70 | |
| ZK9502-03 | 44.00 | | | 12.00 | | 1.20 | | | 18.00 | | 2.50 | 0.30 | 20.40 | 1.60 | |
| ZK9502-04 | 41.30 | | | 34.60 | | | | | 17.20 | | 5.90 | | | 1.10 | |
| ZK9502-05 | 68.00 | | | 15.20 | | | 3.50 | | 6.40 | 4.10 | 2.80 | | | | |
| ZK9502-06 | 53.70 | | | | | 35.60 | 1.40 | | 6.50 | 2.00 | 0.80 | | | | |
| ZK9502-07 | 77.10 | | | | | 11.40 | 1.70 | | 6.70 | 1.80 | 1.30 | | | | |
| ZK9502-08 | 75.90 | | | | | 7.90 | 2.90 | 1.50 | 6.80 | 3.30 | 1.70 | | | | |
| ZK9502-09 | | | | | | 95.50 | 4.50 | | | | | | | | |
| ZK9502-10 | | | | | 68.10 | | 5.90 | | 3.50 | 22.50 | | | | | |
| ZK9502-11 | | 3.10 | | | 51.10 | 27.30 | 8.70 | | 2.70 | 7.30 | | | | | |
| ZK9502-12 | | 39.90 | | | 47.90 | 2.70 | | | 6.60 | | 0.50 | | | 2.50 | |
| ZK9502-13 | | 44.60 | | | 33.50 | 10.40 | 4.30 | | 4.30 | | 1.90 | | | 1.10 | |
| ZK9502-14 | | 6.20 | | | 16.40 | 55.00 | 14.70 | | 2.40 | | | | | | 5.30 |
| ZK9502-15 | 3.20 | 8.50 | | | 42.20 | 3.90 | 7.20 | | 8.60 | 23.20 | 0.90 | | | 2.20 | |
| ZK9502-16 | 12.50 | 79.90 | | | 2.40 | 1.00 | | | 3.10 | | 0.50 | | | 0.70 | |
| ZK9502-17 | | 90.00 | 5.20 | | 1.10 | | | | 0.80 | | 1.00 | | 1.90 | | |
| ZK9502-18 | | 87.50 | | | | 1.30 | 1.00 | | 7.70 | | 2.50 | | | | |
| ZK9502-19 | | | | | | 95.60 | 3.00 | | 1.30 | | | | | | |
| ZK9502-20 | | | | | 10.50 | 75.60 | 10.90 | | 1.80 | 1.10 | | | | | |
| ZK9502-21 | | | | | 11.00 | 57.60 | 31.30 | | | | | | | | |
| ZK9502-22 | | | | | 19.50 | 72.60 | 2.70 | | 0.70 | 4.50 | | | | | |
| ZK9502-23 | | | | | 9.10 | 86.70 | 4.00 | | 0.20 | | | | | | |
| ZK9502-24 | | | | | 6.20 | 91.60 | 1.20 | | 1.00 | | | | | | |
| ZK9502-25 | | | | | 12.10 | 84.60 | 1.60 | | 1.80 | | | | | | |
| ZK9502-26 | | | | | 9.40 | 88.40 | 2.10 | | | | | | | | |
| ZK9502-27 | | | | | 16.40 | 80.50 | 3.10 | | | | | | | | |
| ZK9502-28 | | | | | 38.30 | 53.90 | 1.80 | | 1.50 | 4.50 | | | | | |
| ZK9502-29 | | | | | 15.50 | 74.80 | 6.00 | | | 3.70 | | | | | |
| ZK9502-30 | 24.90 | | | | 22.60 | 39.00 | 6.20 | | 1.30 | 6.10 | | | | | |
| ZK9502-31 | | | | | 7.20 | 88.60 | 4.30 | | | | | | | | |
| ZK9502-32 | | | | | 8.20 | 86.20 | 5.60 | | | | | | | | |
| ZK9502-33 | | | | | 1.40 | 95.90 | 2.70 | | | | | | | | |
| ZK9502-34 | 14.20 | | | | 14.10 | 55.60 | 2.10 | | 1.80 | 12.20 | | | | | |
| ZK9502-35 | 16.20 | | | | 17.50 | 44.30 | 2.90 | | 2.20 | 14.20 | | | | 2.70 | |
| ZK9502-36 | 7.10 | | | | 24.10 | 57.30 | 5.90 | | 2.50 | 3.10 | | | | | |

Table 1. Cont.

| Sample | Illite | Kaolinite | Clinochlore | Cookeite | Quartz | Calcite | Dolomite | Siderite | Pyrite | Albite | Anatase | Rutile | Diaspore | Bassanite | Melanterite |
|-----------|--------|-----------|-------------|----------|--------|---------|----------|----------|--------|--------|---------|--------|----------|-----------|-------------|
| ZK9502-37 | | | | | 30.30 | 66.60 | 3.10 | | | | | | | | |
| ZK9502-38 | | | | | 2.90 | 90.70 | 6.40 | | | | | | | | |
| ZK9502-39 | | 2.70 | | | 22.00 | 65.20 | 7.60 | | 2.50 | | | | | | |
| ZK9502-40 | | | | | 4.70 | 90.90 | 4.40 | | | | | | | | |
| ZK9502-41 | 9.40 | 5.20 | | | 4.40 | 76.50 | 4.00 | | 0.50 | | | | | | |
| ZK9502-42 | | 85.70 | 6.80 | | | 2.50 | | | 1.90 | | 0.90 | | 2.20 | | |
| ZK9502-43 | | 38.20 | | | 57.00 | 4.10 | | | 0.60 | | 0.10 | | | | |
| ZK9502-44 | | 6.90 | | | 23.40 | 64.10 | 5.10 | | 0.50 | | | | | | |
| ZK9502-45 | | 6.10 | | | | 92.60 | | | 1.30 | | | | | | |
| ZK9502-46 | | 5.40 | | | 4.10 | 79.10 | 9.90 | | 1.50 | | | | | | |
| ZK9502-47 | | | | | | 68.00 | 31.70 | | 0.30 | | | | | | |
| ZK9502-48 | | | | | | 97.10 | 1.40 | | 1.50 | | | | | | |
| ZK9502-49 | | | | | 7.70 | 81.70 | 3.50 | | | 7.20 | | | | | |
| ZK9502-50 | | 3.60 | | | 32.70 | 49.30 | 2.50 | | 0.90 | 10.90 | | | | | |
| ZK9502-51 | | | | | 9.50 | 78.20 | 6.30 | | 0.30 | 5.70 | | | | | |

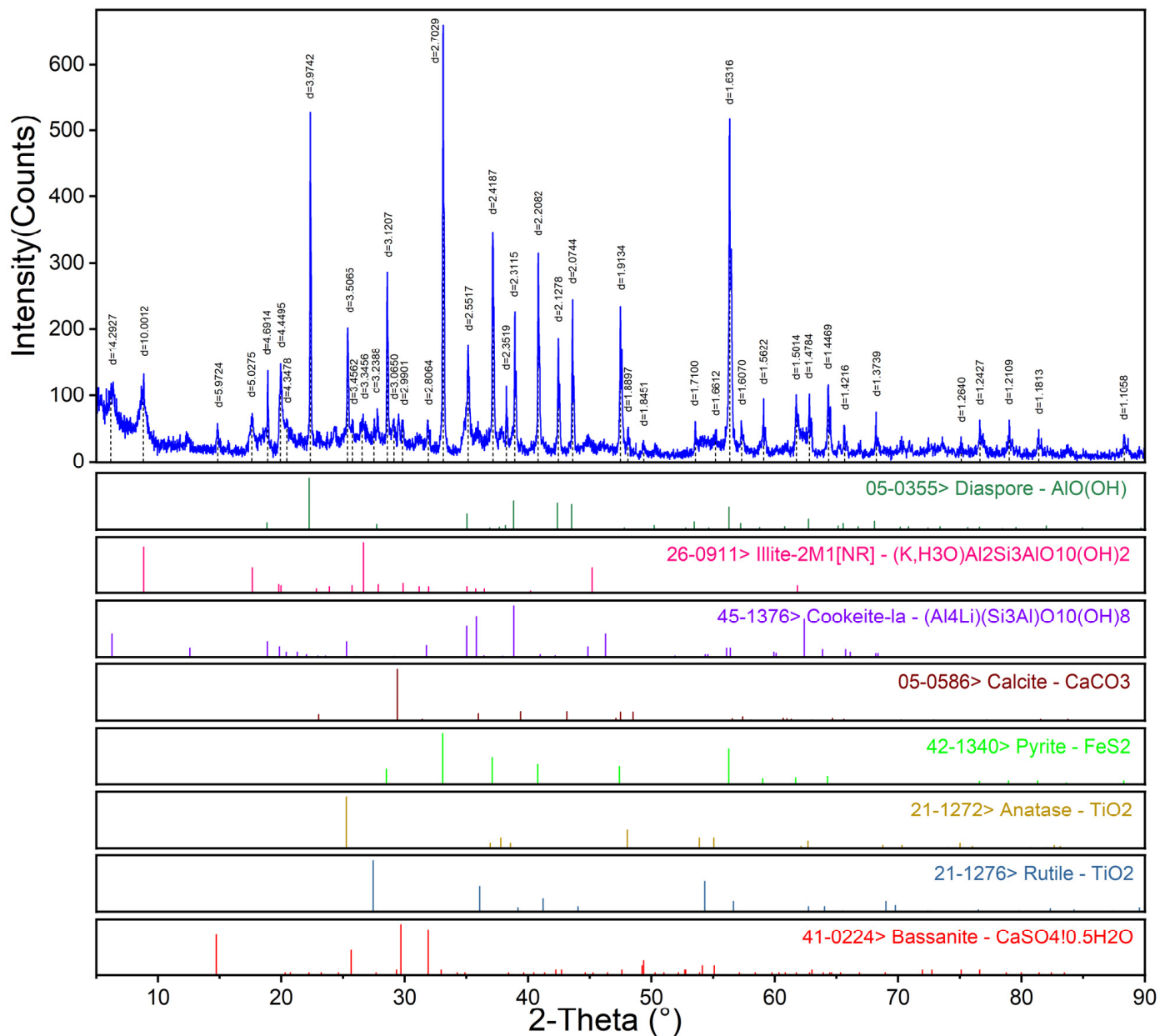


Figure 3. Minerals in ZK9502-03.

4.1.2. Mode of Occurrence of Minerals

Illite primarily occurs as layers along the bedding planes (Figure 4A), and to a lesser extent, in association with kaolinite, occurring as a fine-grained mixture of the two minerals.

Calcite is the dominant mineral in the studied samples; calcite is found as fracture and cavity infillings (Figure 4A,B)

Quartz occurs as independent subhedral to euhedral crystals, indicating that the quartz is of detrital origin (Figure 4A,B and Figure 5A,B).

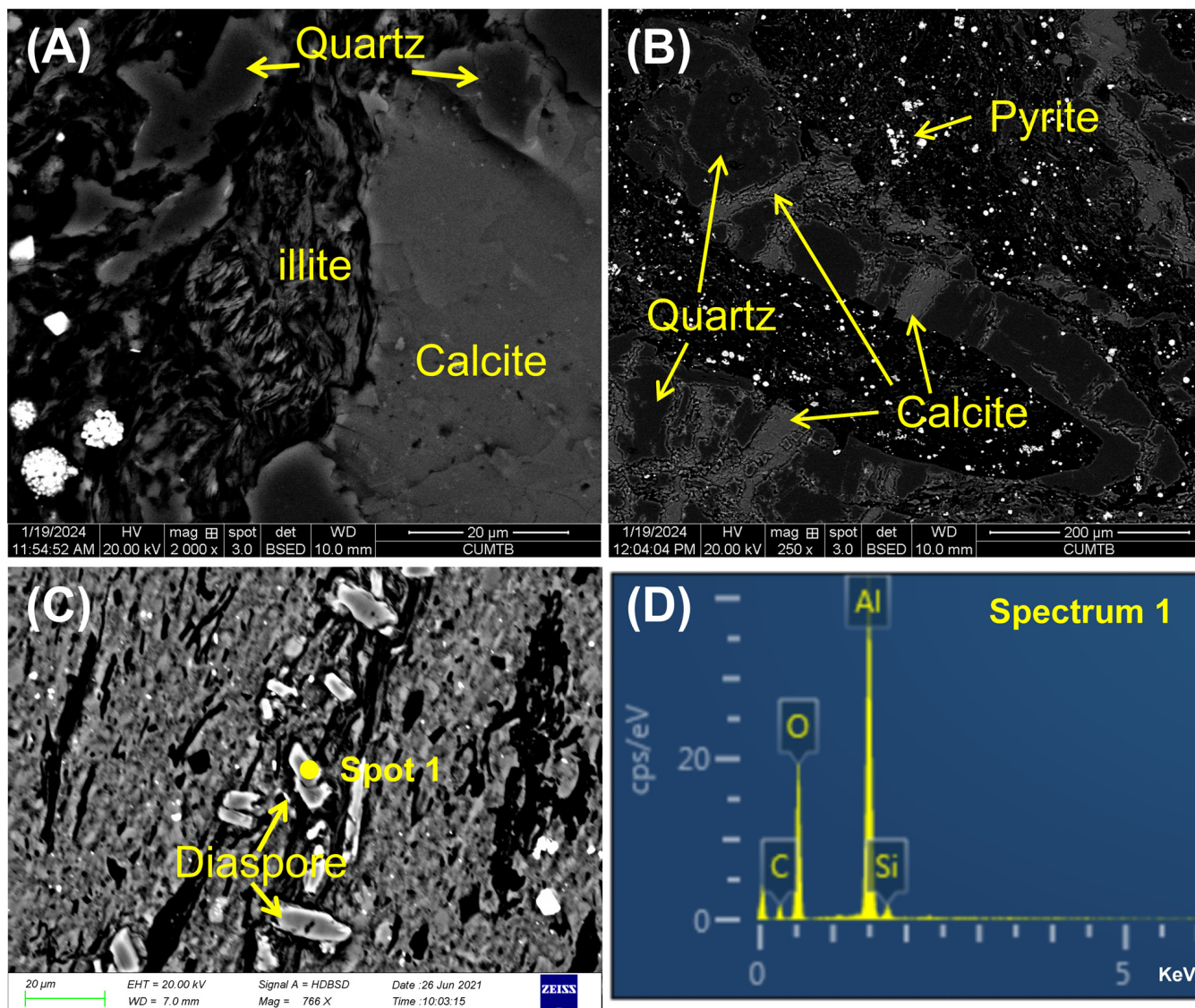


Figure 4. SEM backscattered electron images of minerals in samples. (A) Layers of illite along the bedding planes and particle quartz in sample ZK9502-02; (B) calcite, quartz, and pyrite in sample ZK9502-02; (C) diaspore in sample ZK9502-03; (D) EDS spectrum of diaspore in (C) in sample ZK9502-03.

Pyrite primarily occurs as single euhedral crystals or framboidal pyrite aggregates (Figure 4A,B and Figure 5B,D).

Albite mainly occurs as dispersed particles with irregular corroded borders (Figure 5A), indicating the alteration of albite. Diaspore is also found in some samples and primarily occurs as dispersed particles embedded within a clay minerals matrix (Figure 4C), indicating a detrital origin.

Jarosite, as an iron sulphate mineral, was found in the studied samples using SEM. Rao and Gluskoter [17] reported jarosite is most likely derived from the oxidation of pyrite during storage in the lab. The jarosite was scattered in the corroded pyrite matrix or as the outer part of the corroded pyrite (Figure 5D). Furthermore, the existence of melanterite could also be another piece of evidence for the oxidation of pyrite [18,19].

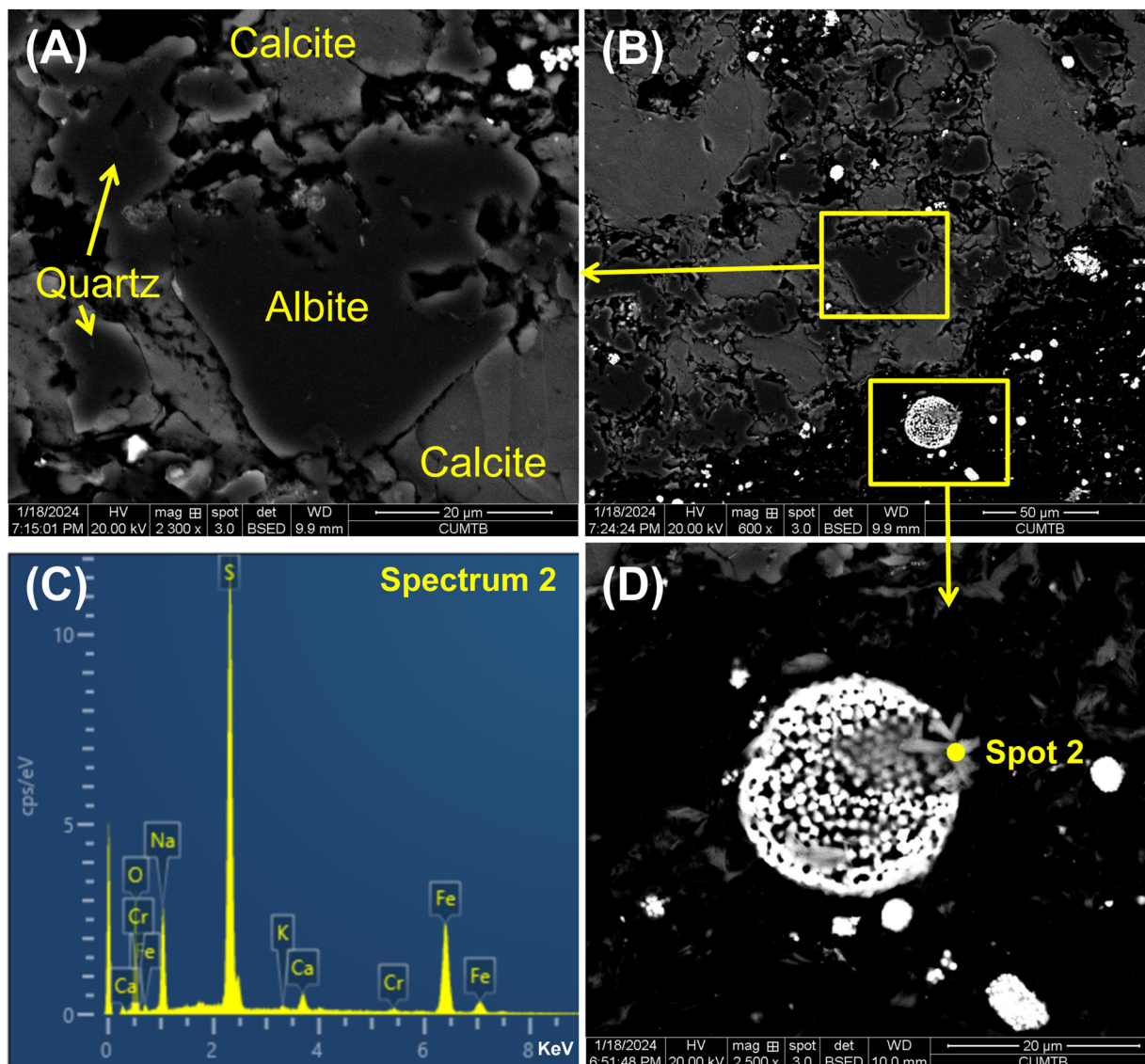


Figure 5. SEM backscattered electron images of minerals in samples. (A) Calcite, quartz, and albite in sample ZK9502-02; (B) calcite, pyrite, quartz, and albite in sample ZK9502-02; (C) EDS spectrum of natrojarosite in (D) in sample ZJ-5-14; (D) pyrite and natrojarosite in sample ZK9502-02.

4.2. Geochemistry

4.2.1. Major Element Oxides

Table 2 provides the concentrations of major element oxides in bench samples. The major element oxides in mineralized layers I, II, III, and IV are SiO₂ and Al₂O₃, which are probably affiliated with clay minerals and feldspars in the samples. The constant elements in the floor and roof of the mineralized layers mainly include CaO and SiO₂, which are consistent with the co-occurrences of calcite–quartz.

The ratio of SiO₂/Al₂O₃ increases sequentially from mineralized layers I to IV, which largely results from the quartz- and Na-bearing feldspars in mineralized layers III and IV. Moreover, the low SiO₂/Al₂O₃ ratio in mineralized layer I can be attributed to the presence of diaspore.

Table 2. The percentage of major element oxides (%) and trace element concentrations in the study samples (µg/g).

| Sample | SiO ₂ | TiO ₂ | Al ₂ O ₃ | Fe ₂ O ₃ | MnO | MgO | CaO | Na ₂ O | K ₂ O | P ₂ O ₅ | Li | Be | Sc | V | Cr | Co | Ni | Cu | Zn | Ga | Rb | Sr | Zr | Nb |
|-----------|------------------|------------------|--------------------------------|--------------------------------|------|------|-------|-------------------|------------------|-------------------------------|---------|------|------|------|------|------|------|------|------|------|------|------|-----|------|
| ZK9502-01 | 0.25 | 0.06 | 0.63 | 1.60 | 0.12 | 1.20 | 50.00 | 0.05 | 0.08 | 0.01 | 5.4 | 0.77 | 1.0 | 54 | 54 | 2.8 | 22 | 5.2 | 39 | 2 | 3.4 | 847 | 21 | 2.8 |
| ZK9502-02 | 11.00 | 0.71 | 10.00 | 18.00 | 0.04 | 0.64 | 7.60 | 0.30 | 0.72 | 0.01 | 357 | 2.6 | 12 | 255 | 177 | 8.6 | 61 | 29 | 43 | 22 | 25 | 222 | 433 | 25 |
| ZK9502-03 | 17.00 | 2.90 | 32.00 | 19.00 | 0.03 | 0.30 | 1.10 | 0.38 | 1.40 | 0.01 | 11945.6 | 23 | 414 | 520 | 9.8 | 42 | 54 | 34 | 52 | 44 | 36 | 703 | 97 | |
| ZK9502-04 | 28.00 | 2.70 | 30.00 | 14.00 | 0.03 | 0.44 | 0.56 | 0.52 | 1.60 | 0.02 | 38537.2 | 24 | 690 | 660 | 108 | 316 | 157 | 57 | 29 | 48 | 39 | 635 | 83 | |
| ZK9502-05 | 34.00 | 2.40 | 30.00 | 11.00 | 0.02 | 0.64 | 0.75 | 0.97 | 2.70 | 0.02 | 20526.2 | 21 | 1133 | 1039 | 79 | 322 | 126 | 76 | 31 | 91 | 53 | 577 | 75 | |
| ZK9502-06 | 26.00 | 1.50 | 22.00 | 9.80 | 0.04 | 0.65 | 15.00 | 1.10 | 1.70 | 0.02 | 739 | 4.1 | 24 | 683 | 839 | 80 | 374 | 77 | 84 | 27 | 60 | 211 | 369 | 49 |
| ZK9502-07 | 32.00 | 2.50 | 24.00 | 11.00 | <dl | 0.94 | 7.80 | 0.30 | 4.10 | 0.02 | 19 | 1.4 | 23 | 389 | 499 | 36 | 138 | 73 | 53 | 35 | 137 | 100 | 539 | 72 |
| ZK9502-08 | 33.00 | 2.50 | 25.00 | 11.00 | <dl | 1.20 | 4.00 | 0.36 | 3.90 | 0.02 | 16 | 1.7 | 26 | 441 | 557 | 36 | 160 | 82 | 62 | 38 | 143 | 66 | 603 | 79 |
| ZK9502-09 | <dl | 0.02 | 0.41 | 0.12 | 0.01 | 1.40 | 49.00 | 0.06 | 0.11 | 0.01 | 11 | 0.11 | 0.61 | 33 | 47 | 3.1 | 16 | 1.3 | 21 | 0.27 | 1.3 | 345 | 6.3 | 0.57 |
| ZK9502-10 | 52.00 | 0.21 | 10.00 | 2.10 | 0.24 | 1.90 | 12.00 | 1.20 | 0.59 | 0.03 | 36 | 1.5 | 6.1 | 69 | 23 | 8.2 | 15 | 9.6 | 45 | 11 | 26 | 1135 | 110 | 7.3 |
| ZK9502-11 | 62.00 | 0.30 | 14.00 | 2.50 | 0.09 | 1.80 | 1.70 | 2.10 | 0.69 | 0.07 | 44 | 2.1 | 7.6 | 86 | 40 | 5.3 | 11 | 7.8 | 45 | 16 | 36 | 581 | 165 | 10 |
| ZK9502-12 | 41.00 | 0.35 | 14.00 | 3.20 | 0.04 | 0.62 | 2.10 | 1.00 | 0.64 | 0.02 | 126 | 1.9 | 10 | 79 | 27 | 7.6 | 13 | 11 | 37 | 18 | 27 | 629 | 235 | 13 |
| ZK9502-13 | 40.00 | 0.45 | 17.00 | 2.80 | 0.03 | 1.20 | 4.50 | 0.82 | 0.73 | 0.02 | 140 | 1.9 | 11 | 96 | 37 | 6.8 | 17 | 10 | 39 | 19 | 30 | 695 | 233 | 13 |
| ZK9502-14 | 28.00 | 0.26 | 11.00 | 1.80 | 0.05 | 3.90 | 23.00 | 1.00 | 0.54 | 0.01 | 33 | 1.7 | 8.6 | 139 | 87 | 7.3 | 24 | 7.2 | 36 | 13 | 19 | 2059 | 148 | 9.3 |
| ZK9502-15 | 46.00 | 0.40 | 17.00 | 3.80 | 0.05 | 1.50 | 2.20 | 1.80 | 1.40 | 0.02 | 34 | 3.0 | 13 | 229 | 141 | 5.2 | 44 | 18 | 107 | 21 | 65 | 1219 | 425 | 24 |
| ZK9502-16 | 34.00 | 0.75 | 26.00 | 3.30 | 0.01 | 0.38 | 0.92 | 0.50 | 0.72 | 0.01 | 426 | 4.2 | 13 | 265 | 346 | 7.2 | 55 | 19 | 59 | 28 | 22 | 225 | 493 | 49 |
| ZK9502-17 | 37.00 | 0.94 | 32.00 | 1.40 | 0.01 | 0.19 | 0.22 | 0.19 | 0.30 | 0.01 | 925 | 4.8 | 10 | 178 | 314 | 7.3 | 52 | 13 | 40 | 26 | 8 | 94 | 580 | 48 |
| ZK9502-18 | 22.00 | 2.30 | 19.00 | 7.30 | <dl | 0.30 | 0.67 | 0.18 | 0.19 | 0.01 | 450 | 5.0 | 27 | 484 | 757 | 70 | 225 | 215 | 69 | 40 | 4.6 | 55 | 680 | 98 |
| ZK9502-19 | 1.00 | 0.08 | 1.50 | 8.50 | 0.05 | 1.40 | 67.00 | 0.11 | 0.20 | 0.01 | 6.9 | 0.48 | 4.9 | 23 | 38 | 4 | 21 | 3.6 | 11 | 1.2 | 0.73 | 584 | 11 | 1.2 |
| ZK9502-20 | 15.00 | 0.13 | 3.30 | 1.80 | 0.05 | 2.90 | 36.00 | 0.76 | 0.27 | 0.05 | 7.9 | 0.87 | 3.9 | 17 | 214 | 4.4 | 15 | 16 | 39 | 5.5 | 8.5 | 1063 | 90 | 3.1 |
| ZK9502-21 | 15.00 | 0.03 | 0.97 | 0.56 | 0.06 | 6.70 | 36.00 | 0.22 | 0.11 | 0.03 | 7.1 | 0.75 | 1.7 | 17 | 228 | 2.3 | 31 | 109 | 15 | 1.3 | 2.3 | 1187 | 27 | 1.2 |
| ZK9502-22 | 26.00 | 0.10 | 2.70 | 1.20 | 0.03 | 1.40 | 35.00 | 0.76 | 0.23 | 0.02 | 6.8 | 0.70 | 2.9 | 47 | 336 | 3.7 | 21 | 10 | 23 | 2.7 | 6.1 | 1638 | 33 | 2.6 |
| ZK9502-23 | 11.00 | 0.05 | 1.30 | 0.37 | 0.01 | 1.50 | 44.00 | 0.21 | 0.12 | 0.01 | 4.6 | 0.28 | 2.6 | 54 | 112 | 2.8 | 22 | 11 | 12 | 1.5 | 4.1 | 2011 | 15 | 1 |
| ZK9502-24 | 8.70 | 0.06 | 1.70 | 0.53 | 0.02 | 0.95 | 44.00 | 0.29 | 0.14 | 0.01 | 6.6 | 0.76 | 2.9 | 28 | 76 | 3.2 | 18 | 5.2 | 13 | 2 | 3.6 | 2685 | 24 | 1.6 |
| ZK9502-42 | 39.00 | 1.10 | 37.00 | 2.70 | 0.02 | 0.23 | 1.40 | 0.28 | 0.26 | 0.01 | 11475.8 | 13 | 123 | 175 | 5.4 | 40 | 13 | 21 | 33 | 5.4 | 140 | 505 | 48 | |
| ZK9502-43 | 72.00 | 0.47 | 14.00 | 1.50 | <dl | 0.19 | 2.20 | 0.31 | 0.26 | 0.01 | 980 | 5.9 | 14 | 122 | 184 | 5.6 | 41 | 13 | 22 | 37 | 5.6 | 145 | 428 | 48 |
| Sample | Cs | Ba | La | Ce | Pr | Nd | Sm | Eu | Gd | Tb | Dy | Y | Ho | Er | Tm | Yb | Lu | Hf | Ta | Tl | Pb | Th | U | |
| ZK9502-01 | 0.66 | 12 | 19 | 32 | 3 | 11 | 2.1 | 0.55 | 2.5 | 0.3 | 1.9 | 29 | 0.37 | 0.96 | 0.12 | 0.67 | 0.09 | 0.61 | 0.22 | 0.74 | 2.9 | 1 | 4.7 | |
| ZK9502-02 | 6.4 | 75 | 35 | 103 | 11 | 50 | 11 | 2.8 | 12 | 2.3 | 15 | 119 | 3.3 | 9.7 | 1.2 | 7.2 | 1.1 | 8.5 | 1.7 | 8 | 15 | 7.4 | 35 | |
| ZK9502-03 | 9.9 | 137 | 35 | 110 | 9.2 | 36 | 9.3 | 2.3 | 10 | 1.8 | 13 | 74 | 3 | 9.3 | 1.3 | 8.2 | 1.3 | 18 | 6.3 | 7 | 50 | 27 | 32 | |
| ZK9502-04 | 12 | 160 | 175 | 417 | 53 | 223 | 46 | 9.1 | 42 | 5.5 | 28 | 125 | 5 | 12 | 1.7 | 10 | 1.5 | 17 | 5.5 | 1.8 | 72 | 26 | 28 | |
| ZK9502-05 | 17 | 314 | 333 | 326 | 90 | 360 | 64 | 12 | 56 | 6.9 | 33 | 147 | 5.8 | 14 | 1.7 | 9.7 | 1.4 | 15 | 4.9 | 1.3 | 58 | 27 | 30 | |
| ZK9502-06 | 11 | 210 | 311 | 185 | 70 | 274 | 43 | 9.1 | 42 | 5.4 | 28 | 132 | 5.1 | 12 | 1.6 | 9.3 | 1.3 | 10 | 3.3 | 2.5 | 39 | 18 | 20 | |
| ZK9502-07 | 19 | 388 | 75 | 149 | 19 | 76 | 15 | 2.8 | 13 | 2.1 | 12 | 62 | 2.4 | 7.2 | 1 | 6.6 | 0.97 | 13 | 4.6 | 2.9 | 33 | 19 | 12 | |
| ZK9502-08 | 18 | 420 | 79 | 175 | 21 | 84 | 17 | 3.3 | 15 | 2.3 | 13 | 69 | 2.7 | 7.9 | 1.2 | 7.4 | 1.1 | 15 | 5.2 | | 45 | 21 | 13 | |

Table 2. Cont.

| Sample | SiO ₂ | TiO ₂ | Al ₂ O ₃ | Fe ₂ O ₃ | MnO | MgO | CaO | Na ₂ O | K ₂ O | P ₂ O ₅ | Li | Be | Sc | V | Cr | Co | Ni | Cu | Zn | Ga | Rb | Sr | Zr | Nb | |
|-----------|------------------|------------------|--------------------------------|--------------------------------|------|-----|------|-------------------|------------------|-------------------------------|------|-----|------|------|------|------|------|------|------|----|-----|------|-----|----|--|
| ZK9502-09 | 0.17 | 6.1 | 1.7 | 2.4 | 0.45 | 1.7 | 0.34 | 0.07 | 0.3 | 0.04 | 0.24 | 2.1 | 0.05 | 0.14 | 0.02 | 0.12 | 0.02 | 0.18 | 0.05 | | 1.8 | 0.28 | 2.3 | | |
| ZK9502-10 | 5.6 | 195 | 20 | 50 | 4.8 | 18 | 4.5 | 0.8 | 4.6 | 0.72 | 4.5 | 25 | 0.88 | 2.7 | 0.4 | 2.6 | 0.39 | 3.6 | 0.77 | | 25 | 12 | 18 | | |
| ZK9502-11 | 11 | 213 | 37 | 75 | 8.3 | 29 | 6.1 | 0.75 | 5.7 | 0.91 | 5.4 | 32 | 1.1 | 3.4 | 0.49 | 3.3 | 0.5 | 5.1 | 1.1 | | 28 | 18 | 19 | | |
| ZK9502-12 | 11 | 88 | 39 | 87 | 10 | 41 | 9.1 | 1.2 | 9 | 1.6 | 10 | 71 | 2.2 | 6.9 | 1 | 6.6 | 1 | 5.6 | 0.99 | | 36 | 15 | 22 | | |
| ZK9502-13 | 12 | 67 | 31 | 69 | 8.4 | 31 | 7.3 | 0.89 | 7 | 1.2 | 7.7 | 51 | 1.6 | 5 | 0.8 | 5.2 | 0.79 | 6.6 | 1.3 | | 40 | 19 | 24 | | |
| ZK9502-14 | 7.5 | 73 | 67 | 101 | 12 | 48 | 11 | 1.8 | 11 | 2 | 12 | 66 | 2.5 | 7.5 | 1.1 | 7 | 0.99 | 4.3 | 0.82 | | 26 | 12 | 11 | | |
| ZK9502-15 | 20 | 204 | 30 | 68 | 8.2 | 30 | 6.9 | 0.84 | 6.4 | 1.2 | 7.6 | 42 | 1.6 | 5.1 | 0.78 | 5.2 | 0.79 | 11 | 1.7 | | 40 | 23 | 55 | | |
| ZK9502-16 | 7.5 | 61 | 54 | 117 | 13 | 52 | 11 | 1.5 | 10 | 1.9 | 11 | 72 | 2.4 | 7.6 | 1.1 | 7.3 | 1.1 | 12 | 3.5 | | 49 | 28 | 51 | | |
| ZK9502-17 | 5.3 | 25 | 48 | 97 | 10 | 40 | 7.9 | 0.95 | 6.6 | 1.1 | 6.5 | 36 | 1.3 | 4 | 0.6 | 3.9 | 0.56 | 16 | 2.6 | | 39 | 31 | 24 | | |
| ZK9502-18 | 4.2 | 31 | 91 | 177 | 25 | 98 | 21 | 4.6 | 18 | 3 | 18 | 65 | 3.5 | 10 | 1.5 | 9.8 | 1.5 | 18 | 6 | | 50 | 24 | 10 | | |
| ZK9502-19 | 0.18 | 8.4 | 24 | 21 | 8.3 | 38 | 10 | 3 | 16 | 2.7 | 16 | 122 | 3.4 | 9.6 | 1.2 | 6 | 0.83 | 0.37 | 0.11 | | 2.1 | 0.4 | 4.9 | | |
| ZK9502-20 | 2.2 | 103 | 8.9 | 18 | 2.5 | 11 | 3 | 0.71 | 3.3 | 0.61 | 3.6 | 23 | 0.8 | 2.3 | 0.38 | 2.3 | 0.35 | 2.1 | 0.2 | | 5.3 | 2.4 | 2.7 | | |
| ZK9502-21 | 0.39 | 21 | 3 | 5.7 | 0.7 | 2.8 | 0.74 | 0.17 | 0.93 | 0.18 | 1.1 | 9.8 | 0.27 | 0.76 | 0.13 | 0.79 | 0.12 | 0.52 | 0.08 | | 2.1 | 0.93 | 3.4 | | |
| ZK9502-22 | 1.1 | 45 | 8.9 | 15 | 1.9 | 7.3 | 1.6 | 0.28 | 1.5 | 0.26 | 1.4 | 11 | 0.32 | 0.9 | 0.14 | 0.86 | 0.13 | 0.69 | 0.15 | | 5.6 | 2.4 | 5.9 | | |
| ZK9502-23 | 0.7 | 26 | 9.2 | 12 | 1.4 | 5.5 | 1.1 | 0.23 | 1.2 | 0.19 | 1 | 9.2 | 0.22 | 0.58 | 0.09 | 0.52 | 0.07 | 0.42 | 0.09 | | 4.2 | 1.5 | 7.8 | | |
| ZK9502-24 | 0.94 | 47 | 14 | 21 | 2.5 | 9.8 | 2.5 | 0.53 | 3.8 | 0.77 | 5.3 | 50 | 1.4 | 3.9 | 0.65 | 3.9 | 0.59 | 0.63 | 0.11 | | 4.2 | 2.1 | 6.3 | | |
| ZK9502-42 | 5.7 | 24 | 29 | 60 | 6.5 | 24 | 4.8 | 0.61 | 4.3 | 0.86 | 5.1 | 31 | 1.1 | 3.2 | 0.53 | 3.3 | 0.49 | 12 | 3.1 | | 52 | 35 | 23 | | |
| ZK9502-43 | 5.8 | 22 | 29 | 61 | 6.7 | 24 | 4.9 | 0.63 | 4.4 | 0.89 | 5.3 | 34 | 1.2 | 3.3 | 0.56 | 3.5 | 0.53 | 13 | 3 | | 55 | 33 | 22 | | |

4.2.2. Trace Elements

The trace element contents of the mineralized layer bench samples collected from the ZK9502 drill hole are listed in Table 2. Figure 6 compares the trace element values of the mineralized layers determined in this study with the average values of the world clay data reported by Grigoriev et al. [20]. The concentration coefficients (CC) of <0.5, 0.5–2, 2.0–5.0, 5.0–10, 10–100, and >100 indicate depleted, similarity, slight enrichment, enrichment, significant enrichment, and unusual enrichment, respectively [21].



Figure 6. Concentration coefficients of trace elements of mineralized layers I, II, III, and IV in coal-bearing series from Wanfu mine, Xian’an coalfield, Guangxi Province.

Lithium is significantly enriched in mineralized layer I, with a CC of >10. The trace elements with a CC of 5–10 include Cr, Nb, Eu, Gd, Er, and U. Other slightly enriched trace elements include V, Co, Ni, Cu, Ga, Y, Zr, La, Ce, Pr, Nd, Sm, Tb, Dy, Ho, Tm, Yb, Lu, Hf, Ta, Tl, and Pb, with CC of 2–5. Only trace elements have a CC of <0.5, which are Rb, Sr, and Ba. Meanwhile, the remaining elements, Be, Sc, Zn, Cs, and Th, with CC of 0.5–2, have concentrations close to the corresponding averages of the upper continental crust (Figure 3).

As shown in Figure 6, compared with the average values of the world clay data, Li, Cr, Cu, Nb, and Er are enriched ($5 < CC < 10$) in mineralized layer II. V, Co, Ni, Ga, Zr, REY (except Eu and Er), Hf, Ta, Pb, and U are slightly enriched ($2 < CC < 5$). Be, Sc, Zn, La, and Th ($0.5 < CC < 2$) are close to the average values of the world clay. Rb, Sr, Cs, and Ba are depleted ($CC < 0.5$).

In mineralized layer III, compared with the average values of the world clay, Li is significantly enriched ($10 < CC < 100$). U is enriched ($5 < CC < 10$). Cr, Zr, Nb, Er, Yb, Lu, Hf, Ta, Pb, and Th are slightly enriched ($2 < CC < 5$). Co, Cu, Zn, Rb, Cs, and Ba are depleted ($CC < 0.5$). The remaining elements are close to the average values of the world clay ($0.5 < CC < 2$) (Figure 6).

In mineralized layer IV, compared with the average values of the world clay, Li, V, Sr, Dy, Ho, Er, Yb, Lu, Pb, and U are slightly enriched ($2 < CC < 5$). Cr, Co, Ni, Cu, Zn, Rb, and Ba are depleted ($CC < 0.5$). The remaining elements are close to the average values of the world clay ($0.5 < CC < 2$) (Figure 6).

The concentration of lithium (Li) ranges from 33 to 133 $\mu\text{g/g}$, with an average value of 88 $\mu\text{g/g}$. The concentration of Ga is between 13 and 20 $\mu\text{g/g}$ and is 17 $\mu\text{g/g}$ on average. REY have a concentration ranging from 230 to 355 $\mu\text{g/g}$ and an average value of 295 $\mu\text{g/g}$. Additionally, the concentration of U varies from 12 to 24 $\mu\text{g/g}$, with a mean value of 19 $\mu\text{g/g}$.

4.2.3. Rare Earth Element and Yttrium (REY)

The total REY concentrations in mineralized layers I, II, III, and IV are 895, 551, 249, and 295 $\mu\text{g/g}$, respectively (Table 2).

The REY enrichment in mineralized layers I and II belong to the H-REY type ($\text{La}_N/\text{Lu}_N < 1$; Figure 7) and M-REY type ($\text{La}_N/\text{Sm}_N < 1$ and $\text{Gd}_N/\text{Lu}_N > 1$), with no or slightly positive Eu anomalies (Figure 7). In mineralized layers III and IV, REY enrichment exhibits the H-REY type ($\text{La}_N/\text{Lu}_N < 1$; Figure 7) and M-REY type ($\text{La}_N/\text{Sm}_N < 1$, $\text{Gd}_N/\text{Lu}_N > 1$), accompanied by varying degrees of negative Eu anomalies, indicating the input of detrital material with a chondrite-like composition [22,23].

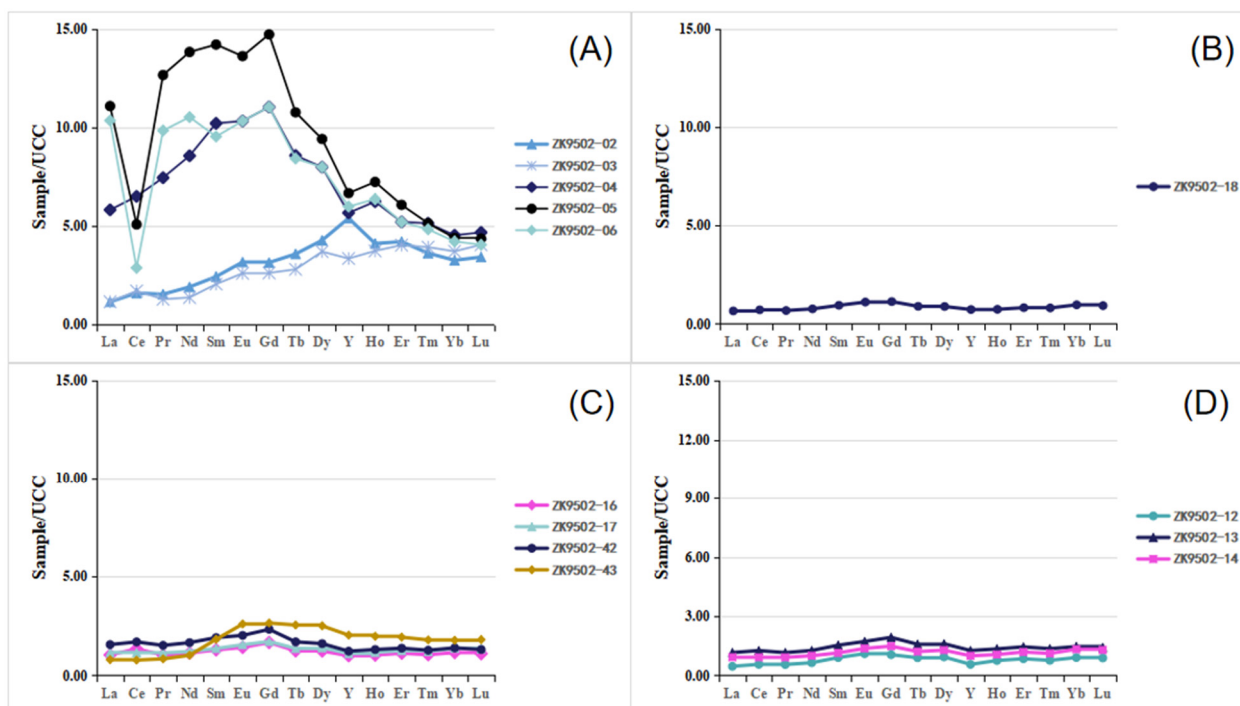


Figure 7. REY distribution patterns of mineralized layers I (A), II (B), III (C), and IV (D) in coal-bearing series from Wanfu mine, Xian'an coalfield, Guangxi Province. REY are normalized to Upper Continental Crust (UCC) [22].

5. Discussion

5.1. Sediment Source Region

The ratio of $\text{Al}_2\text{O}_3/\text{TiO}_2$ in sedimentary rocks generally corresponds to the lithology of the source rock, which is effective for determining the properties of source rocks [24]. Girty et al. (1996) suggested that a $\text{Al}_2\text{O}_3/\text{TiO}_2$ ratio between 3 and 8 indicated a predominantly mafic igneous rock, a ratio from 8 to 21 implied a chiefly intermediate igneous rock, and a ratio between 21 and 70 mainly represented a felsic igneous rock [25].

The ratios of $\text{Al}_2\text{O}_3/\text{TiO}_2$ in the samples in mineralized layers I and II indicate that the sediment source region is mainly characterized by intermediate igneous rocks, while the ratios of $\text{Al}_2\text{O}_3/\text{TiO}_2$ in the samples in mineralized layers III and IV denote that the sediment source region has the characteristic of felsic igneous rocks (Figure 8). Previous studies demonstrated that the dominant source region of sediment in the late Permian coal-bearing strata in Guangxi Province, China was the detrital material derived from weathering residues located immediately above the Maokou Formation limestone [26–28]. These residues primarily consist of terrigenous felsic detrital materials. Hence, the terrigenous materials for the mineralized layers in the Wanfu mine stem from the continental detrital material of the Daxin upland. Additionally, volcanic detrital material induced by the Emeishan mantle plume and the northern magmatic arc also significantly influences the composition of these strata [29,30].

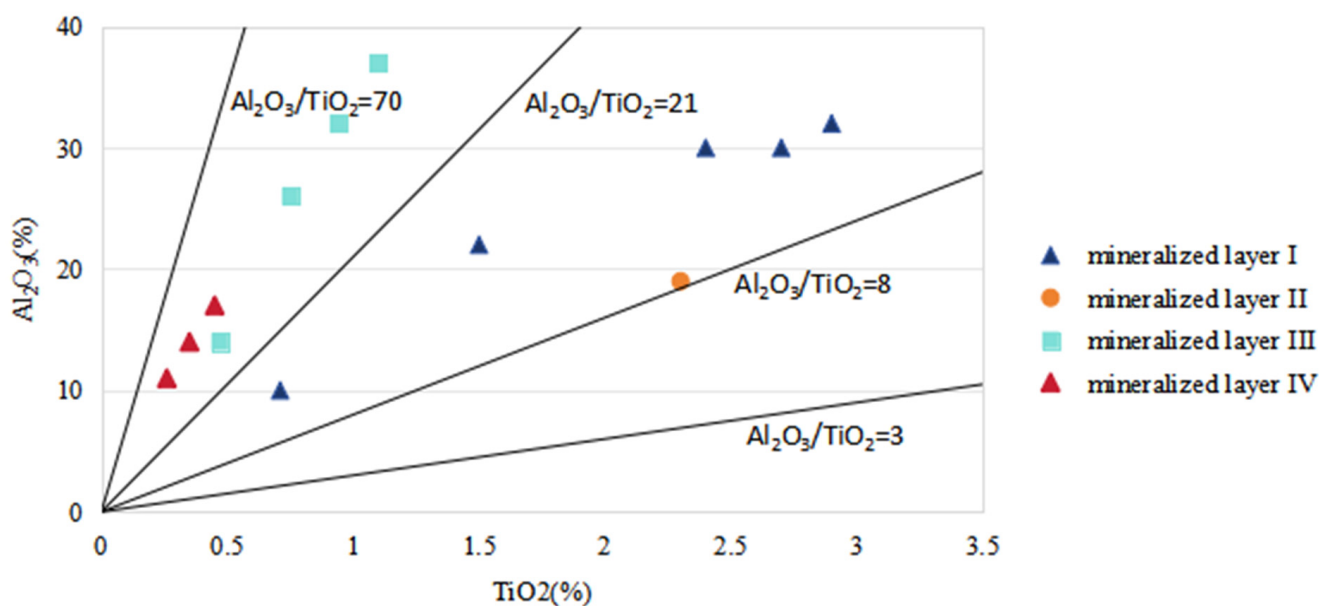


Figure 8. Plot of TiO_2 vs. Al_2O_3 in the samples from the mineralized layers I, II, III, and IV in the coal-bearing strata from the Wanfu mine, Xian'an coalfield, Guangxi Province.

According to the La/Sc-Th/Co diagram proposed by Cullers (2000) [31], most sample points are in the felsic igneous rock region, with a few points from mineralized layers I and II falling outside the region (Figure 9). Therefore, the mineralized layers in the Heshan Formation in Guangxi mainly originate from intermediate and felsic igneous rocks.

5.2. Volcanic Ash

By plotting the samples of coal-bearing Li ore layers I, II, III, and IV from Wanfu mine, Xian'an Coalfield in Guangxi onto the Nb/Y-Zr/TiO₂ provenance discrimination diagram (Figure 10), it can be observed that the sample points mainly fall within the fields of coarse-grained andesite, coarse-grained rock, andesite, and rhyolite, which partially overlap with the late-stage felsic igneous rocks in the Emeishan large igneous province. From this, it is inferred that the late-stage felsic igneous rock in the Emeishan large igneous

province may be one of the sources of Li ore layers I, II, III, and IV in the Wanfu mine, Xian'an Coalfield, Guangxi [32–34].

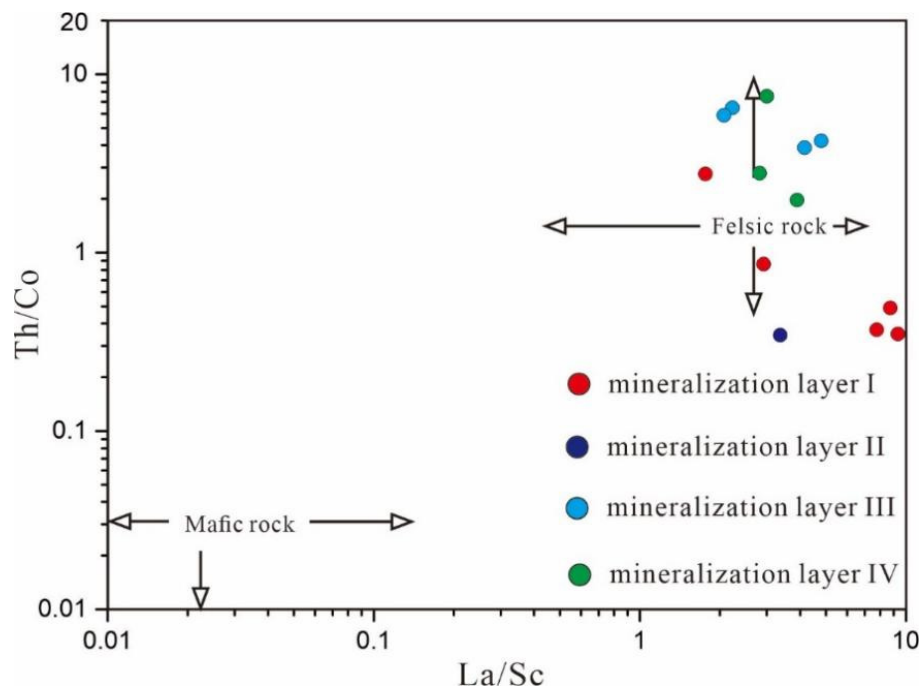


Figure 9. Plot of La/Sc-Th/Co in the samples in mineralized layers I, II, III, and IV in the coal-bearing strata from the Wanfu mine, Xian'an coalfield, Guangxi Province.

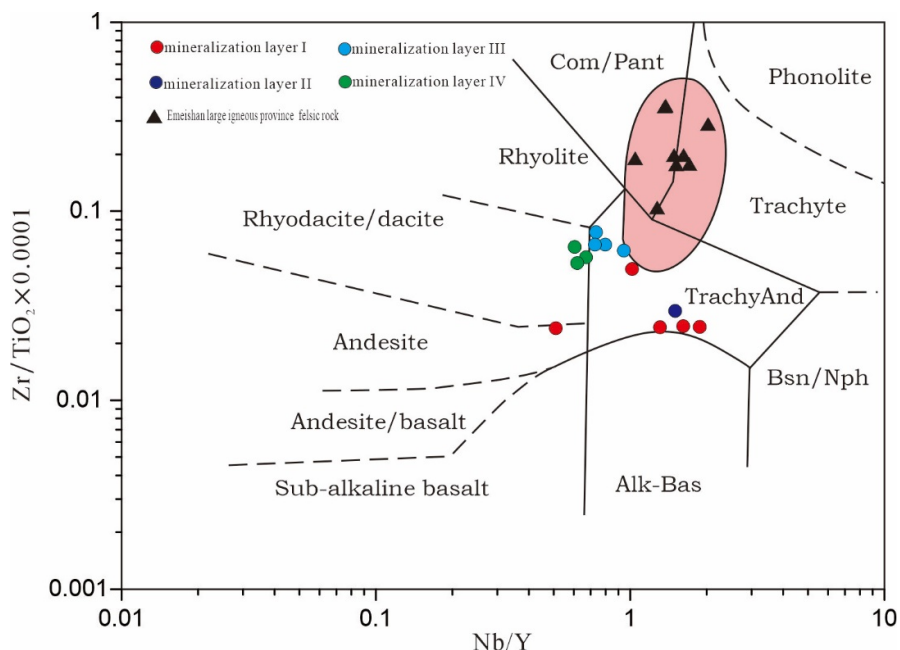


Figure 10. Plot of Nb/Y-Zr/TiO₂ in the samples from the mineralized layers I, II, III, and IV in the coal-bearing strata from the Wanfu mine, Xian'an coalfield, Guangxi Province.

Additionally, Zhang et al. [35] conducted a thorough analysis using zircon U-Pb dating, zircon trace elements Th/Nb-Hf/Th and Th/U-Nb/Hf tectonic discrimination diagrams, and rare earth elements. This analysis suggests that the lithium mineralization layers in the Heshan Formation of Guangxi are primarily derived from intermediate to felsic igneous

rocks related to the Emeishan large igneous province and the Permian magmatic arc of the Paleo-Tethys.

5.3. Hydrothermal Fluids

Previous studies have indicated that the differentiation of Eu in surface environments is challenging due to the stringent requirements for high reducing conditions (stronger than SO_4^{2-} - H_2S) and elevated temperatures ($>250^\circ\text{C}$) [36]. Typically, Eu anomalies are inherited from the source rock [37]. For instance, detrital material derived from the Emeishan basalt in the Late Permian coals of the Qiannan region exhibits a positive Eu anomaly in its upper crust-normalized rare earth element distribution [38,39]. Geochemical indicators such as $\text{Al}_2\text{O}_3/\text{TiO}_2$ -Th/Sc diagrams, Zr/ TiO_2 -Nb/Y diagrams, and the vertical distribution of $\text{Al}_2\text{O}_3/\text{TiO}_2$ collectively suggest that the detrital material in mineralized layer I of borehole ZK9502 has an intermediate to acidic composition. Consequently, a negative Eu anomaly is expected in this layer. However, conversely, a slightly positive Eu anomaly (1.06–1.13) is observed.

Positive Eu anomalies are commonly associated with high-temperature hydrothermal fluids affecting coal deposits and mafic volcanic ash, as well as being inherited from sediment source rocks with a mafic-dominated composition [40–42]. The sediment source region of mineralized layer I was mainly characterized by intermediate–felsic igneous composition, and, therefore, the minor positive Eu anomaly in this layer may be attributed to the influence of hydrothermal fluids. Furthermore, the consistency of the positive Eu anomaly in mineralized layer I suggests that the input of hydrothermal fluids may have occurred during the syn- to early-diagenetic stages when hydrothermal fluids could more easily permeate the mineralized layer.

6. Conclusions

Four Li-Ga-REY enriched mineralized layers are developed in the coal-bearing strata in Wanfu mine, Xian'an Coalfield, Guangxi Province. Mineralized layers I, II, III, and IV correspond to the coal layers K5, K4, K3, and K2 in the coal-bearing strata of the Heshan Group, respectively. The enrichment mineralization of Li, Ga, and REY in the mineralized layers stems from the combination of intermediate–felsic-dominated composition sediment source inputs, intermediate–felsic volcanic ash inputs, and hydrothermal fluids occurring during the syn- to early-diagenetic stages.

Author Contributions: Conceptualization, D.Z., X.Y. and B.L.; methodology, X.Y.; software, B.L.; J.S. and L.Z. collected the samples; X.Y., X.J., X.X., S.D. and S.H. conducted the experiments; D.Z., X.Y. and X.J., writing—original manuscript; B.L. and J.S. revised the manuscript. All authors have read and agreed to the published version of the manuscript.

Funding: This research was supported by The National Key R&D Program of China (2021YFC2902005), the National Natural Science Foundation of China (No.42102211, 42272207), and the China Coal Geological Administration Carbon Neutral Special Project (ZMKJ-2021-ZX03).

Data Availability Statement: Data are contained within the article.

Acknowledgments: The authors would like to give their sincere thanks to the Guangxi Bureau of Coal Geology for assistance during sampling and to Fuqiang Zhang (Guangxi Bureau of Coal Geology) for his great help in the analysis of data.

Conflicts of Interest: The authors declare no conflicts of interest.

References

1. Hou, Z.; Chen, J.; Zhai, M. Current status and frontiers of research on critical mineral resources. *Chin. Sci. Bull.* **2020**, *65*, 3651–3652. [[CrossRef](#)]
2. Mao, J.; Zeng, Z.; Li, T.; Yuan, S.; Xie, G.; Song, S.; Zhou, Q.; Gao, Y.; Liu, X.; Fu, X.; et al. New advances on metallogenic studies and exploration on critical minerals of China in 21st century. *Miner. Depos.* **2019**, *38*, 935–969.
3. Zhai, M.; Wu, F.; Hu, R.; Jiang, S.; Li, W.; Wang, R.; Wang, D.; Qi, T.; Qin, K.; Wen, H. Critical metal mineral resources: Current situation and problems. *Sci. Found. China* **2019**, *33*, 106–111.

4. Wang, D. Research significance of key minerals, determination of mineral species, resource properties, prospecting progress, existing problems and main direction of attack. *Acta Geol. Sin.* **2019**, *93*, 1189–1209.
5. Seredin, V.; Dai, S.; Sun, Y.; Chekryzhov, I.Y. Coal deposits as promising sources of rare metals for alternative power and energy-efficient technologies. *Appl. Geochem.* **2013**, *31*, 1–11. [[CrossRef](#)]
6. Dai, S.; Liu, C.; Zhao, L.; Liu, J.; Wang, X.; Ren, D. Stratagic Metal Resources in Coal-bearing Strata: Significance and Challenges. *J. China Coal Soc.* **2022**, *47*, 1743–1749.
7. Dai, S.; Zhao, L.; Wei, Q.; Song, X.L.; Wang, W.F.; Liu, J.J.; Duan, P.P. Resources of critical metals in coal-bearing sequences in China: Enrichment types and distribution. *Chin. Sci. Bull.* **2020**, *65*, 3715–3729. (In Chinese) [[CrossRef](#)]
8. Dai, S.; Yan, X.; Ward, C.; Hower, J.C.; Zhao, L.; Wang, X.; Zhao, L.; Ren, D.; Finkelman, R.B. Valuable elements in Chinese coals: A review. *Int. Geol. Rev.* **2018**, *60*, 590–620. [[CrossRef](#)]
9. Liao, J.; Zhang, F.; Wei, M.; Liang, X. Lithium and gallium abundance and enrichment factors in typical Late Permian coal accumulation basins in Guangxi. *Coal Geol. Explor.* **2020**, *48*, 77–84.
10. Dai, S.; Zhang, W.; Seredin, V.V.; Ward, C.R.; Hower, J.C.; Song, W.; Wang, X.; Li, X.; Zhao, L.; Kang, H.; et al. Factors controlling geochemical and mineralogical compositions of coals preserved within marine carbonate successions: A case study from the Heshan Coalfield, southern China. *Int. J. Coal Geol.* **2013**, *109*, 77–100. [[CrossRef](#)]
11. Shao, L.; Jones, T.; Gayer, R.; Dai, S.; Li, S.; Jiang, Y.; Zhang, P. Petrology and geochemistry of the high-sulphur coals from the Late Permian carbonate coal measures in the Heshan Coalfield, southern China. *Int. J. Coal Geol.* **2003**, *55*, 1–26. [[CrossRef](#)]
12. Dai, S.; Zhang, W.; Ward, C.R.; Seredin, V.V.; Hower, J.C.; Li, X.; Song, W.; Wang, X.; Kang, H.; Zheng, L.; et al. Mineralogical and geochemical anomalies of late Permian coals from the Fusui Coalfield, Guangxi Province, southern China: Influences of terrigenous materials and hydrothermal fluids. *Int. J. Coal Geol.* **2013**, *105*, 60–84. [[CrossRef](#)]
13. Zhang, F.; Li, B.; Zhuang, X.; Querol, X.; Moreno, N.; Shangguan, Y.; Zhou, J.; Liao, J. Geological Controls on Enrichment of Rare Earth Elements and Yttrium (REY) in Late Permian Coals and Non-Coal Rocks in the Xian'an Coalfield, Guangxi Province. *Minerals* **2021**, *11*, 301. [[CrossRef](#)]
14. Zhou, H. *Permian System in Guangxi*; China University of Geosciences Press: Wuhan, China, 2014.
15. Zhang, P.; Shao, L. Sedimentary facies zones and sedimentary models of Heshan Formation, Heshan Area, Guangxi. *Acta Sedimentol. Sin.* **1990**, *8*, 9.
16. Wang, G.; Wen, X. Sedimentary facies analysis of Late Permian Heshan Formation in Guangxi. *Curr. Geol.* **1995**, *1*, 119–127.
17. Karayigit, A.; Bircan, C.; Oskay, R.; Türkmen, I.; Querol, X. The geology, mineralogy, petrography, and geochemistry of the Miocene Dursunbey coal within fluvio-lacustrine deposits, Balikesir (Western Turkey). *Int. J. Coal Geol.* **2020**, *228*, 103548. [[CrossRef](#)]
18. Kortenski, J.; Sotirov, A. Petrography of the Neogene lignite from the Sofia basin, Bulgaria. *Int. J. Coal Geol.* **2004**, *57*, 117–126. [[CrossRef](#)]
19. Rao, C.; Gluskoter, H. Occurrence and distribution of minerals in Illinois coals. *Ill. State Geol. Surv. Circ.* **1973**, *476*, 56.
20. Grigoriev, N. *Chemical Element Distribution in the Upper Continental Crust*; UBRAS: Ekaterinburg, Russia, 2009; p. 382. (In Russian)
21. Dai, S.; Seredin, V.; Ward, C.; Hower, J.C.; Xing, Y.; Zhang, W.; Song, W.; Wang, P. Enrichment of U–Se–Mo–Re–V in coals preserved within marine carbonate successions: Geochemical and mineralogical data from the Late Permian Guiding Coal-field, Guizhou, China. *Miner. Depos.* **2015**, *50*, 159–186. [[CrossRef](#)]
22. Taylor, S.R.; McLennan, S.M. *The Continental Crust: Its Composition and Evolution*; Blackwell: Hoboken, NJ, USA, 1985; p. 312.
23. Seredin, V.; Dai, S. Coal deposits as potential alternative sources for lanthanides and yttrium. *Int. J. Coal Geol.* **2012**, *94*, 67–93. [[CrossRef](#)]
24. Hayashi, K.; Fujisawa, H.; Holland, H.; Ohmoto, H. Geochemistry of ~1.9 Ga sedimentary rocks from northeastern Labrador, Canada. *Geochim. Cosmochim. Acta* **1997**, *61*, 4115–4137. [[CrossRef](#)] [[PubMed](#)]
25. Girty, G.; Ridge, D.; Knaack, C.; Johnson, D.; Al-Riyami, R.K. Provenance and depositional setting of Paleozoic chert and argillite, Sierra Nevada, California. *J. Sediment. Res.* **1996**, *66*, 107–118.
26. Li, B.; Zhang, F.; Liao, J.; Li, B.; Zhuang, X.; Querol, X.; Moreno, N.; Shangguan, Y. Geological Controls on Geochemical Anomaly of the Carbonaceous Mudstones in Xian'an Coalfield, Guangxi Province, China. *Energies* **2022**, *15*, 5196. [[CrossRef](#)]
27. Cao, B.; Qin, Y.; Zhu, S.; Fu, X.; Xu, H.; Zong, S. Origin and enrichment mechanism of lithium and rare earth elements in carbonaceous mudstone of Heshan Formation, Shanglin, Guangxi. *J. China Coal Soc.* **2022**, *47*, 1851–1864.
28. Liao, J.; Wei, M.; Liang, X. Analysis on Late Permian Heshan Formation Coal Accumulation Basin Lithium Resource Features in Guangxi. *Coal Geol. China* **2020**, *32*, 1674–1803.
29. Dai, S.; Liu, J.; Ward, C.; Hower, J.C.; French, D.; Jia, S.; Hood, M.M.; Garrison, T.M. Mineralogical and geochemical compositions of Late Permian coals and host rocks from the Guxu Coalfield, Sichuan Province, China, with emphasis on enrichment of rare metals. *Int. J. Coal Geol.* **2016**, *166*, 71–95. [[CrossRef](#)]
30. Yang, T.; Shen, Y.; Lu, L.; Jin, J.; Huang, W.; Li, F.; Zhang, Y.; Hu, J.; Zeng, L. Geological factors for the enrichment of critical elements within the Lopingian (Late Permian) coal-bearing strata in western Guizhou, Southwestern China: Constrained with whole-rock and zircon geochemistry. *Int. J. Coal Geol.* **2024**, *282*, 104441. [[CrossRef](#)]
31. Cullers, R. The geochemistry of shales, siltstones and sandstones of Pennsylvanian–Permian age, Colorado, USA: Implications for provenance and metamorphic studies. *Lithos* **2000**, *51*, 181–203. [[CrossRef](#)]

32. Hei, H.; Su, S.; Wang, Y.; Mo, X.X.; Luo, Z.H.; Liu, W.G. Rhyolites in the Emeishan large igneous province (SW China) with implications for plume-related felsic magmatism. *J. Asian Earth Sci.* **2018**, *164*, 344–365. [[CrossRef](#)]
33. Xu, Y.; Chung, S.; Shao, H.; He, B. Silicic magmas from the Emeishan large igneous province, Southwest China: Petrogenesis and their link with the end-Guadalupian biological crisis. *Lithos* **2010**, *119*, 47–60. [[CrossRef](#)]
34. Hoa, T.; Anh, T.; Phuong, N.; Dung, P.T.; Anh, T.V.; Izokh, A.E.; Borisenko, A.S.; Lan, C.Y.; Chung, S.L.; Lo, C.H. Permo-Triassic intermediate-felsic magmatism of the Truong Son belt, eastern margin of Indochina. *C. R. Geosci.* **2008**, *340*, 112–126. [[CrossRef](#)]
35. Zhang, D.; Xu, X.; Sun, J.; Li, B.; Zhang, L.; Zhuang, X.; Yan, X. Geochemical characteristics and provenance of lithium in the Late Permian Heshan Formation coal-bearing series from the Wanfu mining area, Shanglin, Guangxi Province. *J. China Coal Soc.* **2023**, *1178*.
36. Bau, M.; Moeller, P. Rare earth element fractionation in metamorphogenic hydrothermal calcite, magnesite and siderite. *Mineral. Petrol.* **1992**, *45*, 231–246. [[CrossRef](#)]
37. Dai, S.; Li, D.; Chou, C.; Zhao, L.; Zhang, Y.; Ren, D.; Ma, Y.; Sun, Y. Mineralogy and geochemistry of boehmite-rich coals: New insights from the Haerwusu Surface Mine, Jungar Coalfield, Inner Mongolia, China. *Int. J. Coal Geol.* **2008**, *74*, 185–202. [[CrossRef](#)]
38. Li, B.; Zhuang, X.; Li, J.; Querol, X.; Font, O.; Moreno, N. Geological controls on mineralogy and geochemistry of the Late Permian coals in the Liulong Mine of the Liuzhi Coalfield, Guizhou Province, Southwest China. *Int. J. Coal Geol.* **2016**, *154*, 1–15. [[CrossRef](#)]
39. Li, B.; Zhuang, X.; Li, J.; Querol, X.; Font, O.; Moreno, N. Enrichment and distribution of elements in the Late Permian coals from the Zhina Coalfield, Guizhou Province, Southwest China. *Int. J. Coal Geol.* **2017**, *171*, 111–129. [[CrossRef](#)]
40. Michard, A.; Albarede, F.; Michard, G.; Minster, J.F.; Charlou, J.L. Rare-earth elements and uranium in high-temperature solutions from East Pacific Rise hydrothermal vent field (13N). *Nature* **1983**, *303*, 795–797. [[CrossRef](#)]
41. Michard, A. Rare earth element systematics in hydrothermal fluids. *Geochim. Cosmochim. Acta* **1989**, *53*, 745–750. [[CrossRef](#)]
42. Migdisov, A.; Williams, A.; Brugger, J.; Caporuscio, F.A. Hydrothermal transport, deposition, and fractionation of the REY: Experimental data and thermodynamic calculations. *Chem. Geol.* **2016**, *439*, 13–42. [[CrossRef](#)]

Disclaimer/Publisher’s Note: The statements, opinions and data contained in all publications are solely those of the individual author(s) and contributor(s) and not of MDPI and/or the editor(s). MDPI and/or the editor(s) disclaim responsibility for any injury to people or property resulting from any ideas, methods, instructions or products referred to in the content.